

# Tilt mode stability scaling in field-reversed configurations with finite Larmor radius effect

Naotaka Iwasawa<sup>a)</sup> and Akio Ishida

*Department of Environmental Science, Faculty of Science, Niigata University, Ikarashi, Niigata 950-2181, Japan*

Loren C. Steinhauer

*University of Washington, Redmond Plasma Physics Laboratory, Redmond, Washington 98052*

(Received 27 May 1999; accepted 15 November 1999)

The marginal stability of a static plasma with finite-Larmor-radius (FLR) effects depends on a combination of the FLR effect and the ideal magnetohydrodynamic (MHD) potential energy. For the tilt mode in a field-reversed configuration (FRC) previous computations of these two factors led to a prediction of stability for  $S_* \leq (3-5)E$  where  $S_*$  is the macroscale parameter (separatrix radius/ion skin depth) and  $E$  is the elongation (separatrix half length/separatrix radius). This prediction explained the observed stability of most experiments. However, recent computations of actual MHD eigenfunctions indicate that the MHD growth rate has a much weaker scaling with elongation than previously believed. As a consequence, most of the long-lived, stable FRC experiments lie in the region predicted to be unstable. It appears then that the stability of FRC experiments is not explained by FLR effects in a static equilibrium. © 2000 American Institute of Physics. [S1070-664X(00)00803-X]

## I. CONVENTIONAL CALCULATIONS OF TILT STABILITY

Field-reversed configurations (FRCs) have proved grossly stable with lifetimes limited by the resistive decay of the magnetic configuration. The notable exception is a rotational mode that can be stabilized by weak multipole fields. By now it is accepted that the explanation for this lies outside the standard magnetohydrodynamic (MHD) model applied to static equilibria. The stability has usually been ascribed to ion finite-Larmor-radius (FLR) effects. The most feared mode, because of its potential for disrupting confinement, is the tilt mode. The FLR effect on tilting has been modeled using gyroviscous<sup>1,2</sup> as well as hybrid models (kinetic ions, fluid electrons).<sup>3-5</sup> The fluid-based gyroviscous model is particularly useful for determining marginal stability conditions because it can give the actual eigenvalues of the mode while requiring only modest computations.

The dispersion relation for a static equilibrium including FLR effects is

$$\omega^2 + C_{\text{FLR}}\Omega_*\omega + \gamma_{\text{MHD}}^2 = 0, \quad (1)$$

where  $\gamma_{\text{MHD}}$  is the ideal MHD growth rate. The middle term is the FLR effect:  $\Omega_*$  is the drift frequency, and  $C_{\text{FLR}}$  is a coefficient of order unity which depends on the particular mode and the equilibrium. The  $C_{\text{FLR}}$  and  $\gamma_{\text{MHD}}$  are routinely computed for the tilt mode in FRC using the gyroviscous model. This has been done by solving the equivalent variational problem<sup>1</sup> using the Rayleigh–Ritz technique.<sup>1,2</sup> A small basis set of three elements was used for the displace-

ment vector field; the basis elements were chosen intuitively. These results predicted an ideal MHD growth rate of roughly

$$\gamma_{\text{MHD}} \approx V_{A0}/aE, \quad (2)$$

where  $a$  is the separatrix radius,  $V_{A0} = B_e/(4\pi\rho_m)^{1/2}$  is the reference Alfvén speed (based on the external field  $B_e$  and the maximum density  $\rho_m$ ) and  $E$  is elongation=separatrix length-to-diameter ratio. For typical FRCs the drift frequency is  $\Omega_* \approx V_{A0}l_r/a^2$ , where  $l_r = c/\omega_{pi}$  is the ion skin depth (based on the maximum density). From typical results<sup>2</sup>  $C_{\text{FLR}} \approx 5$ . Combining these, FLR stability (non-negative discriminant) is achieved if

$$S_* \leq 3E. \quad (3)$$

It has been observed that the stability of nearly all FRC experiments could be explained if the constant of proportionality in Eq. (3) was in the neighborhood of 5. Approximate but more insightful models have yielded similar results.<sup>6</sup> In short then, the FLR theory of static equilibria gave a reasonable explanation for the tilt stability of FRCs.

## II. MHD GROWTH RATE WITH TRUE EIGENVECTORS

Recently, the algorithm for a Rayleigh–Ritz solution to the variational problem has been improved to allow a large basis set. This improvement allows the completeness of the basis set to be verified by a convergence test. Applying this to the ideal MHD problem has allowed computation of growth rates for actual eigenmodes of ideal MHD.<sup>7</sup> In MHD the growth rate is  $\gamma^2 = -W/D$ . The inertia is  $D = \int d\tau \rho |\xi|^2$ :  $\rho$  is the mass density;  $\xi$  is the displacement vector field; and the integral is over the system volume. The MHD potential energy is  $W = \int d\tau w$ , where the integrand (potential energy density) can be expressed in various ways.

<sup>a)</sup>Graduate School of Science and Technology.

TABLE I. FRC data digest.

Device/log	$p_0$ (mtorr)	$\bar{n}/10^{15} \text{ cm}^{-3}$	$T_i$ (eV)	$T_e$ (eV)	$r_c$ (cm)	$r_s$ (cm)	$l_s$ (cm)	$\tau_\phi$ ( $\mu\text{sec}$ )	$\tau_{Ep}$ ( $\mu\text{sec}$ )	$\tau_N$ ( $\mu\text{sec}$ )
FRX-B #1	17	3.3	310	100	12.5	5.4	70	50	52	39
FRX-C #1	5	1.9	800	175	25	9	130	250	60	67
FRX-C #2	20	4.7	250	100	25	10	150	180	135	155
LSM #1	2	0.69	670	165	35	16	109	144	57	161
LSM #2	3	0.78	516	154	35	15.2	143	210	79	175
LSM #3	4	1.1	431	140	35	16.6	133	157	78	160
LSM #4	3	0.83	443	120	35	11.1	152	120	42	106
LSM #5	3	0.72	521	158	35	15.4	144	214	82	185
LSM #6	3	0.60	582	194	35	18.6	132	132	69	181
TRX-1 #1	10	3.4	450	...	12.5	6.3	45	75	45	75
TRX-1 #2	15	3.7	350	...	12.5	7	52	85	68	100
TRX-1 #3	20	6.6	300	...	12.5	4.2	53	35	30	55
TRX-2 #1	3	2.4	500	...	12	4.8	51	20	21	50
TRX-2 #2	7	6.4	750	...	12	3.8	33	20	13	20
TRX-2 #3	7	4.9	900	...	12	4.6	29	27	21	29
TRX-2 #4	10	7.4	550	...	12	4.4	33	30	24	37
TRX-2 #5	11	8	475	...	12	4.1	38	30	25	35
TRX-2 #6	10	4.8	550	...	12	4.8	41	25	23	35
TRX-2 #7	10	4.3	400	...	12	5.2	41	32	27	85
TRX-2 #8	12	6	400	...	12	4.7	40	40	34	65
TRX-2 #9	12	2.1	225	...	12	7	63	57	62	130
TRX-2 #10	15	5.2	225	...	12	5.3	60	68	47	87
TRX-2 #11	20	4.8	150	...	12	5.6	66	85	53	80
TRX-2 #12	15	5.4	310	...	12.5	6.8	69	80	...	171
TRX-2 #13	20	7.5	165	...	12.5	7.3	56	90	...	252
OCT #1	...	1.8	200	...	6.5	4.6	150	150	70	100
PIACE #1	...	2.2	250	100	7.4	4.7	80	70	...	53
PIACE #2	...	5.2	580	150	7.4	3.2	80	51	...	42
NUCTE #1	...	6.2	190	...	17	6.8	45	...	...	...
NUCTE #2	10	2.6	280	...	17	5.7	70	80	...	80
FIX #1	...	0.07	68	...	40	14	310	...	...	220
LSX #1	0.7	0.9	1500	500	45	14.3	135	135	63	110
LSX #2	0.7	0.95	1800	...	45	12.4	120	100	...	70
LSX #3	1.3	1.1	1300	...	45	14.8	140	115	65	170
LSX #4	2.5	1.4	950	300	45	15	150	160	100	220
LSX #5	5	1.8	430	175	45	14	260	300	155	280
LSX #6	1.3	0.9	560	...	45	17.5	170	180	114	250
LSX #7	2.5	1	400	...	45	15.8	260	185	110	170
LSX #8	4.5	1.4	300	...	45	17.8	340	360	180	600
LSX #9	5.5	1.5	280	...	45	19	310	450	245	650
LSX #10	5.8	1.1	300	...	45	21.8	380	475	240	550
LSX #11	8	1.3	280	...	45	24	380	535	345	685

For example, for FRCs (no current term) and incompressible modes ( $\nabla \cdot \xi = 0$ ),  $w = w_Q + w_p$ . The pressure drive term is (Ref. 8, Eq. 5)

$$w_p = -ilp'(\psi)\mathbf{B} \cdot (\xi \times \xi^*) - p''(\psi)|\xi \cdot \nabla \psi|^2, \quad (4)$$

and the magnetic compressibility term is  $w_Q = |\nabla \times (\xi \times \mathbf{B})|^2 / 4\pi$ . Here  $\psi$  is the magnetic flux function,  $\mathbf{B}$  is the magnetic field,  $p$  is the pressure, and the prime denotes the derivative. Based on the new computational results,<sup>7</sup>  $w_p$  is the dominant part of  $w$ .

The scaling of  $W_p/D$  with elongation  $E$  is an important question. This scaling has been investigated for various examples of FRC equilibria.<sup>7</sup> Two examples are shown in Fig. 1: (1) *Elliptic/flat* equilibria have elliptic separatrix shape, and flat current profile ( $j_\theta/r = \text{const}$ ). (2) *Racetrack/flat* equilibria have racetrack separatrix shape (relatively straight sides with roughly circular shape near the ends) and flat current profile. The figure shows the dependence of  $W_p/D$  on

elongation. The elliptic/flat equilibria has the scaling  $W_p/D \propto E^{-7/4}$ . This is roughly consistent with the approximate prediction of the growth rate [Eq. (2)] that leads to the familiar FLR stability prediction [Eq. (3)]. However, the racetrack/flat equilibria shows a quite different tendency: while  $W_p/D$  falls at first for increasing  $E$ , it levels off for  $E > 3$ . This difference arises from changes in the structure of  $\xi(r, z)$ . In elliptic/flat equilibria the displacements spread more or less evenly throughout the entire region inside the separatrix. This broadly spread structure occurs for any elongation. In contrast, in racetrack/flat equilibria with  $E > 3$ , the displacements concentrate within about one or two plasma radii of the ends. As a result, the inertia  $D$  does not continue to increase as  $E$  increases; consequently  $W_p/D$  (and  $W/D$ ) levels off.

Further computations<sup>7</sup> show that equilibria with hollow current profile ( $j_\theta/r$  has a minimum near the magnetic axis)

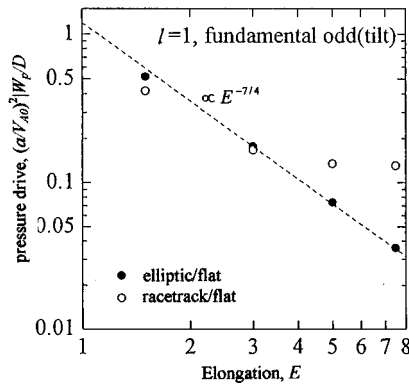


FIG. 1. Elongation scaling for the tilt mode for elliptic and racetrack separatrix shapes. All examples have flat current profile.

exhibit the same trend as the racetrack example in Fig. 1. This is true for both *elliptic/hollow* and *racetrack/hollow* equilibria. Based on inferences from measurements, most experiments are characterized by hollow current profile.<sup>9</sup> Thus the stability scaling [Eq. (3)] of elliptic/flat equilibria appears to be *atypical*. An approximate scaling expression that takes into account the leveling off with larger elongation would be

$$\begin{aligned}
 S_* &\leq 3E; & E < 3, \\
 S_* &\leq 9; & E > 3.
 \end{aligned}
 \tag{5}$$

### III. COMPARISON WITH EXPERIMENTAL DATA

The significance of the corrected  $S_* - E$  scaling becomes apparent in reviewing the experimental data base (see Table I). Figure 2 is an  $S_*$  vs.  $E$  diagram showing the corrected FLR stability prediction [Eq. (5)] as a solid line. Also shown are experimental examples taken from a compendium of long-lived, stable FRCs (see the Appendix). Nearly all experimental examples fall in the regime predicted to be un-

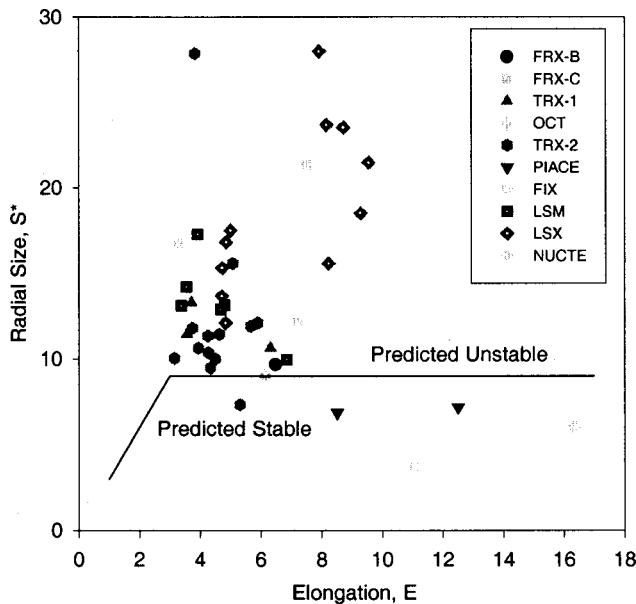


FIG. 2. Tilt stability diagram comparing the corrected gyroviscous theory (solid line) with the experimental data compendium.

stable by the corrected theory, which is a marked change from the earlier understanding.<sup>2,6</sup> It now appears that the FLR of static FRC theory *does not* account for the observed stability. This result was found by making corrections in the MHD potential energy; it needs to be confirmed by applying the Rayleigh–Ritz/variational algorithm to the full gyroviscous model. In any case, it would appear that the tilt stability of FRCs depends on additional effects not included in the FLR static equilibrium theory.

### ACKNOWLEDGMENTS

This work was supported by the Ministry of Education, Science and Culture and by the Collaborating Research Program of the National Institute for Fusion Science, Japan (NI and AI), and U.S. Department of Energy, Grant No. DE-FG03-98ER54480 (LCS).

### APPENDIX: FRC DATA COMPENDIUM

Table I shows a compendium of data from several FRC experiments. It extends a small compendium assembled earlier with a number of new data.<sup>10</sup> Its purpose is to facilitate the comparison of experiment with theories that predict gross plasma behavior, e.g., confinement times. The data set contains only results from FRCs formed in  $\theta$ -pinch facilities. Each record is for “well-behaved” experimental conditions, i.e., results that could be achieved repeatedly for a given set of experimental settings. In most cases a record represents the *average* of results for a given setting. The data base is limited to quiescent examples, excluding instances of continued dynamical behavior due to a protracted formation phase or a rapid postformation relaxation. The time interval to which the quoted quantities apply varies from one record to another. Some examples have shaped coils or mirrors at the ends, which affect the equilibrium. All examples but one have a deuterium plasma. Other specifics are as follows. FRX-B #1 is from Ref. 10, while  $T_i$ ,  $T_e$  are from Ref. 11. FRX-C #1 and 2 are from Ref. 10, while  $T_e$  is from Ref. 11. FRX-C/LSM (denoted as “LSM”) #1–3 are from Ref. 12; #4–6 are from Ref. 13. In all “LSM” examples  $l_s$  is inferred from the quoted  $r_s$  and plasma volume  $V_p$  using the relation  $V_p = \pi r_s^2 l_s$ . In all “LSM” examples the quoted values for  $\tau_{EP}$  are actually for  $\tau_E$ , i.e., the work done by the external field on the plasma is accounted for. TRX-1 #1–3 are from Ref. 10. TRX-2 #1–11 are from Ref. 10, while #12 and 13 are from Ref. 14; #13 is the lone example using hydrogen. OCT #1 is from Ref. 15. PIACE-II (denoted as “PIACE”) #1 and 2 are from Ref. 16. NUCTE #1 is from Ref. 17, and #2 is from Ref. 18. FIX #1 is from Ref. 19. LSX #1–11 are from Ref. 20.

The *log* number is for reference and does not represent a “shot” number. The *filling pressure*  $p_0$  is only reported for examples using a quasi-static initial fill of molecular deuterium (or hydrogen). The *external magnetic field* is  $B_e$ . The *total temperature*,  $T_t$ , is inferred from pressure balance ( $kT_t = B_e^2 / 2\mu_0 n_m$ ); the average density  $\bar{n}$  is generally inferred in experiment using interferometer signals  $\int n dx$  in combination with excluded flux probes; the peak density  $n_m$  is inferred from it using the relationship  $\bar{n} = n_m(1 - r_s^2/5r_c^2)$

which is valid for rigid-rotor-like profiles. The *electron temperature*  $T_e$  is only reported when it was measured by Thomson scattering. The *coil radius* is  $r_c$ : in one instance (TRX-1) an effective value (larger than the actual coil radius) is used to correct for significant external inductance. The *separatrix radius*  $r_s$  is assumed equal to the measured excluded flux radius at the midplane. The *separatrix length*  $l_s$  is usually inferred from an axial array of excluded flux probes. The *poloidal flux decay time*  $\tau_\phi$  is inferred assuming a rigid-rotor-like internal profile. The *energy decay time*  $\tau_{Ep}$  is inferred from the time history of  $B_e$ ,  $r_s$  and  $l_s$ ; it differs from the actual energy loss time because the effect of work on the plasma boundary is ignored. The *particle inventory decay time*,  $\tau_N$ , is inferred from the time histories of interferometer signals,  $r_s$ ,  $l_s$  and excluded flux radius, and the decay rates of  $\int n dx$ ,  $r_s$ , and  $l_s$ .

<sup>1</sup>L. C. Steinhauer and A. Ishida, Phys. Fluids B **2**, 2422 (1990).

<sup>2</sup>A. Ishida, A. Kanno, and L. C. Steinhauer, Phys. Fluids B **4**, 1280 (1992).

<sup>3</sup>Z. Mikic and E. C. Morse, Phys. Fluids **30**, 2806 (1987).

<sup>4</sup>R. Horiuchi and T. Sato, Phys. Fluids B **2**, 2652 (1990).

<sup>5</sup>K. Nishimura, R. Horiuchi, and T. Sato, Phys. Plasmas **4**, 4035 (1997).

<sup>6</sup>H. Ji, M. Yamada, R. Kulsrud, N. Pomphrey, and H. Himura, Phys. Plasmas **5**, 3685 (1998).

<sup>7</sup>N. Iwasawa, A. Ishida, and L. C. Steinhauer, "Ideal Magnetohydrodynamic Stability of Static Field Reversed Configurations," to appear in J. Phys. Soc. Jpn. (2000).

<sup>8</sup>R. Kanno, A. Ishida, and L. C. Steinhauer, J. Phys. Soc. Jpn. **64**, 463 (1995).

<sup>9</sup>L. C. Steinhauer and A. Ishida, Phys. Fluids B **4**, 645 (1992).

<sup>10</sup>A. L. Hoffman and J. T. Slough, Nucl. Fusion **26**, 1693 (1986).

<sup>11</sup>R. E. Siemon, W. T. Armstrong, D. C. Barnes *et al.*, Fusion Technol. **9**, 13 (1986).

<sup>12</sup>D. J. Rej, G. A. Barnes, M. H. Baron, R. E. Chrien, S. Okada, R. E. Siemon, D. P. Taggart, M. Tuszewski, R. B. Webster, and B. L. Wright, Nucl. Fusion **30**, 1087 (1990).

<sup>13</sup>D. J. Rej, G. A. Barnes, M. H. Baron, R. E. Chrien, S. Okada, R. E. Siemon, D. P. Taggart, M. Tuszewski, R. B. Webster, and B. L. Wright, Phys. Fluids B **2**, 1706 (1990).

<sup>14</sup>J. T. Slough and A. L. Hoffman, Nucl. Fusion **28**, 1121 (1988).

<sup>15</sup>M. Tanjyo, S. Okada, Y. Ito, M. Kako, S. Ohi, S. Goto, T. Ishimura, H. Ito, Y. Nogi, S. Shimura, T. Ikawa, and S. Hamada, in *Plasma Physics and Controlled Nuclear Fusion Research*, Proceedings 10th Conference, London, 1984 (International Atomic Energy Agency, Vienna, 1985), Vol. 2, p. 523.

<sup>16</sup>S. Okada, Y. Kiso, S. Goto, and T. Ishimura, Phys. Fluids B **1**, 2422 (1989).

<sup>17</sup>T. Ishimura, Y. Ueda, S. Sugimoto, S. Okada, Y. Ito, S. Ohi, S. Goto, T. Takahashi, S. Shimamura, Y. Nogi, and S. Hamada, in *Plasma Physics and Controlled Nuclear Fusion Research*, Proceedings 12th Conference, Nice, 1988 (International Atomic Energy Agency, Vienna, 1989), Vol. 2, p. 705.

<sup>18</sup>M. Urano, Y. Ohkuma, T. Takahashi, K. Suzuki, and Y. Nogi, J. Phys. Soc. Jpn. **64**, 4077 (1995).

<sup>19</sup>T. Ohtsuka, M. Okubo, S. Okada, and S. Goto, Phys. Plasmas **5**, 3649 (1998).

<sup>20</sup>J. T. Slough, E. A. Crawford, A. L. Hoffman, R. D. Milroy, R. Maqueda, and G. A. Wurden, in *Plasma Physics and Controlled Nuclear Fusion Research*, Proceedings 14th IAEA Conference, 1992 (International Atomic Energy Agency, Vienna, 1993), Vol. 2, p. 627.